

Responses of ocean circulation and carbon cycle to changes in the position of the Southern Hemisphere westerlies at Last Glacial Maximum

Christoph Völker¹ and Peter Köhler¹

Received 26 August 2013; revised 14 November 2013; accepted 15 November 2013; published 19 December 2013.

[1] We explore the impact of a latitudinal shift in the westerly wind belt over the Southern Ocean on the Atlantic meridional overturning circulation (AMOC) and on the carbon cycle for Last Glacial Maximum background conditions using a state-of-the-art ocean general circulation model. We find that a southward (northward) shift in the westerly winds leads to an intensification (weakening) of no more than 10% of the AMOC. This response of the ocean physics to shifting winds agrees with other studies starting from preindustrial background climate, but the responsible processes are different. In our setup changes in AMOC seemed to be more pulled by upwelling in the south than pushed by downwelling in the north, opposite to what previous studies with different background climate are suggesting. The net effects of the changes in ocean circulation lead to a rise in atmospheric $p\text{CO}_2$ of less than 10 μatm for both northward and southward shift in the winds. For northward shifted winds the zone of upwelling of carbon- and nutrient-rich waters in the Southern Ocean is expanded, leading to more CO_2 outgassing to the atmosphere but also to an enhanced biological pump in the subpolar region. For southward shifted winds the upwelling region contracts around Antarctica, leading to less nutrient export northward and thus a weakening of the biological pump. These model results do not support the idea that shifts in the westerly wind belt play a dominant role in coupling atmospheric CO_2 rise and Antarctic temperature during deglaciation suggested by the ice core data.

Citation: Völker, C., and P. Köhler (2013), Responses of ocean circulation and carbon cycle to changes in the position of the Southern Hemisphere westerlies at Last Glacial Maximum, *Paleoceanography*, 28, 726–739, doi:10.1002/2013PA002556.

1. Introduction

[2] Natural variations in the global carbon cycle leave their imprints in the concentration of CO_2 in the atmosphere. From Antarctic ice cores that record atmospheric $p\text{CO}_2$ over the last 800 kyr [Lüthi *et al.*, 2008] we know that the glacial/interglacial rise in CO_2 is of the order of 80–100 μatm and its temporal changes are highly correlated with Antarctic temperature on both orbital and millennial time scales [e.g., Ahn and Brook, 2008; Fischer *et al.*, 2010; Parrenin *et al.*, 2013]. This correlation of CO_2 and Antarctic temperature has led to various hypotheses which suggest Southern Ocean processes as causes for a dominant

part of the observed deglacial rise in atmospheric CO_2 [e.g., Köhler *et al.*, 2005; Tschumi *et al.*, 2011]. The Southern Ocean is indeed a very important part of the global carbon cycle. For the present day it is a pathway for a major part of anthropogenic carbon uptake in the ocean and has thus changed from a natural CO_2 source to a contemporary CO_2 sink [Gruber *et al.*, 2009].

[3] One hypothesis [Toggweiler *et al.*, 2006] proposes that changes in the Southern Hemispheric (SH) belt of westerly winds are the cause for a dominant part of the observed deglacial CO_2 rise. The reasoning of Toggweiler *et al.* [2006] is based on the fact that nowadays Southern Hemispheric westerly winds lead to the upwelling of carbon-rich waters via a northward Ekman transport. If this westerly-induced upwelling is reduced (either by a northward shift or a reducing of the strength of the westerlies), less carbon-rich water is brought to the surface. As a consequence, net oceanic carbon uptake would drag CO_2 from the atmosphere to the surface of the Southern Ocean, where it would finally be transported to the abyss with deep waters formed around Antarctica. Toggweiler *et al.* [2006] argued about latitudinal shifts in the wind belt (equatorward during colder climates) while they performed simulation scenarios in which the strength, not the position of the SH westerly winds, was modified under the assumption that the effect of both on

¹Alfred Wegener Institute Helmholtz Centre for Polar and Marine Research, Bremerhaven, Germany.

Corresponding author: P. Köhler, Alfred Wegener Institute Helmholtz Centre for Polar and Marine Research, PO Box 120161, D-27515 Bremerhaven, Germany. (peter.koehler@awi.de)

©2013. The Authors.

This is an open access article under the terms of the Creative Commons Attribution-NonCommercial-NoDerivs License, which permits use and distribution in any medium, provided the original work is properly cited, the use is non-commercial and no modifications or adaptations are made. 0883-8305/13/10.1002/2013PA002556

Table 1. Overview Over the Model Runs Presented in This Study

Name	Description
CORE	reference run
LGM	LGM reference run
Shift10S	as LGM and 10° southward shift of SH winds
Shift5S	as LGM and 5° southward shift of SH winds
Shift5N	as LGM and 5° northward shift of SH winds
Shift10N	as LGM and 10° northward shift of SH winds

atmospheric CO₂ might be similar. As already pointed out by *Menviel et al.* [2008], the original article of *Toggweiler et al.* [2006] neither did capture sea ice dynamics properly nor did they consider a primary production consistent with the modified circulation. Furthermore, *Toggweiler et al.* [2006] applied a model with very simplified bathymetry and distribution of continents.

[4] The impact of this “westerly wind hypothesis” has been tested in the meantime by various simulation studies using Earth System Models of Intermediate Complexity. Both the Bern3D model [*Tschumi et al.*, 2008] and the LOVECLIM model [*Menviel et al.*, 2008] did not support the hypothesis that shifts in the westerly wind belt have a substantial impact on atmospheric CO₂. In Bern3D an equatorward shift of westerly winds led to a rise, not a fall, in atmospheric CO₂. Furthermore, *Tschumi et al.* [2008] concluded that SH westerly winds have only a limited impact on atmospheric CO₂ on glacial/interglacial time scales. In LOVECLIM results are also opposite to those proposed by the hypothesis, mainly caused by variability in the biological pump. In a third study using the UVic model [*d’Orgeville et al.*, 2010] it is found that latitudinal shifts in wind and changes in their amplitude—synonymously used in *Toggweiler et al.* [2006]—impact very differently on the carbon cycle and atmospheric CO₂. Most recently, the MESMO model was applied to the same question [*Lee et al.*, 2011] and found some supporting evidence for the hypothesis, with a rise in atmospheric *p*CO₂ by 20 (variable biological pump) to 60 (constant biological pump) μ atm for a southward shift in the SH westerlies.

[5] A number of further studies have investigated the impact of changes in the westerly wind on ocean circulation, without following the link to the carbon cycle [e.g., *Sijp and England*, 2008, 2009; *Delworth and Zeng*, 2008;

Wei et al., 2012]. They all clearly found a connection of Southern Ocean westerly winds (strength and/or latitudinal position) with the meridional overturning circulation in the Atlantic (AMOC) and Pacific Ocean. *Sijp and England* [2008, 2009] even propose that this connection might be the cause for a reduced glacial AMOC. All these studies—testing the hypothesis directly or only the connection of SH westerly winds with AMOC—started from preindustrial or modern background conditions.

[6] The question if and by how much the Southern Ocean westerlies might have been different during the Last Glacial Maximum (LGM) compared to preindustrial climate is not finally resolved until now. Paleoclimate Modelling Intercomparison Project (PMIP) phase 2 simulations indicate that there was no latitudinal shift in the westerly wind belt, but three out of four models found decreased intensities of the near-surface winds [*Rojas et al.*, 2009]. A more recent paleodata synthesis comes to the conclusion that an overall strengthening, a northward shift, or no change at all in winds would all be consistent with reconstructions [*Kohfeld et al.*, 2013]. However, the most likely change in the Southern Ocean westerlies might have been either a small northward displacement by 3–5° or a slight strengthening, but it was emphasized in *Kohfeld et al.* [2013] that a southward shift or a weakening cannot be ruled out based on paleodata alone.

[7] Here we provide another sensitivity test of the westerly wind hypothesis in which various shortcomings of the original study or its successors are overcome: We used a (1) full ocean general circulation model (ocean GCM) (2) including a fully prognostic sea ice model and applied (3) LGM background conditions using (4) a realistic bathymetry. In doing so, the potential role of the different carbon pumps on atmospheric CO₂ can be elucidated. In detail, we shifted the Southern Ocean westerly winds both southward and northward by up to 10°.

2. Methods

2.1. Physical Model

[8] We used the ocean GCM of the Massachusetts Institute of Technology, the MITgcm [*Marshall et al.*, 1997; *MITgcm Group*, 2013], including a state-of-the-art sea ice model [*Losch et al.*, 2010], the KPP turbulent mixing scheme [*Large et al.*, 1994], the Gent-McWilliams parametrization

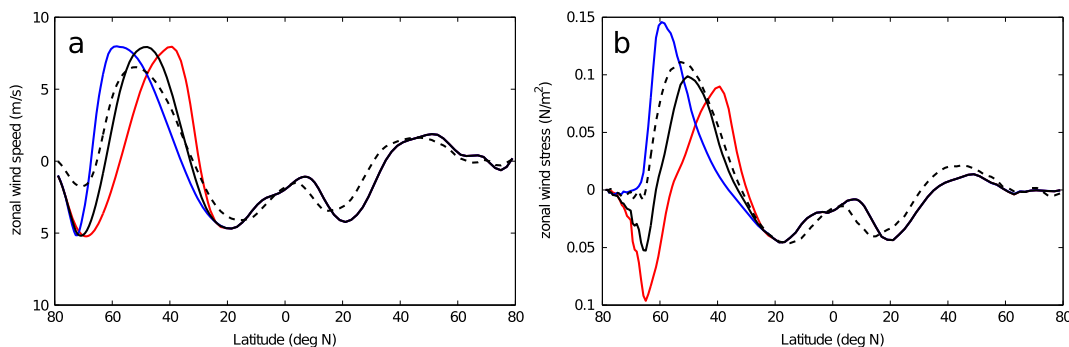


Figure 1. (a) Zonally averaged 10 m zonal wind speed. (b) Zonally averaged zonal wind stress, including the effect of sea ice cover. CORE (dashed line) LGM (solid lines), where black indicates runs without latitudinal shift in the location of the maximum zonal wind stress, red indicates a 10° northward shift, and blue a 10° southward shift. Model runs with $\pm 5^\circ$ shift have been omitted for clarity.

of subgrid-scale eddy fluxes [Gent *et al.*, 1995], and a parametrization of density-driven downslope flows [Campin and Goosse, 1999]. The horizontal resolution is 2° (longitude) \times $(0.38 - 2^\circ)$ (latitude). Highest latitudinal resolution is obtained in our region of interest, the Southern Ocean, and in a belt around the equator. In the vertical we use 30 layers with layer thickness increasing from 10 m at the ocean surface to 500 m in the deep ocean.

[9] Air-sea fluxes of heat, freshwater, and momentum are calculated from bulk formulae [Large *et al.*, 1994], using 2 m atmospheric temperature and relative humidity, 10 m winds, downward shortwave and longwave energy fluxes and precipitation, and continental river runoff. For the LGM simulations, monthly averaged atmospheric forcing fields were taken from coupled atmosphere-ocean simulations performed with COSMOS [Zhang *et al.*, 2013]. Depending on the initial conditions, these authors find two different quasi-stationary states at LGM which differ mainly in the strength of the AMOC. Here we use output from the more stable state with weaker AMOC, called LGMW in Zhang *et al.* [2013]. For a modern control run (CORE) daily varying temperature, winds, and energy fluxes were used from the CORE-1 climatology [Large and Yeager, 2008]. To avoid a drift of the sea surface salinity a weak restoring (time scale of 1 year) of the surface salinity field to either the coupled model run (LGM) or the World Ocean Atlas (CORE) was applied.

2.2. Biogeochemical Model

[10] The biogeochemical model used here, the dissolved inorganic carbon (DIC) package of the MITgcm [Parekh *et al.*, 2006], describes production and export of organic matter as a function of available phosphate, light, and temperature. A constant fraction of the organic matter production is converted to dissolved organic phosphorus that is then remineralized to phosphate at a temperature-dependent rate. The vertical sinking flux of organic matter is assumed to decrease with depth following a simple scaling law [Martin *et al.*, 1987], and the divergence of the flux is treated as a source of phosphate. A constant carbon:phosphorus ratio is assumed for organic matter, and production of CaCO₃ is assumed to be in constant proportion to the production of organic carbon. The ocean is coupled to a homogeneously mixed atmospheric box to account for carbon transfers between atmosphere and ocean.

[11] Our main aim here was to investigate the reaction of the marine carbon cycle to changes in the physical forcing connected with a shift in the position of the SH westerlies, not to reproduce as closely as possible a glacial carbon cycle. There are clearly many more processes that affect the ocean carbon cycle over glacial-interglacial time scales, which are not depicted here (see section 4 for a brief discussion). To focus on the physical effects alone, we deliberately tried to keep these other factors constant. We therefore did not take into account a limitation of the export production through iron, unlike Parekh *et al.* [2006].

2.3. Initialization

[12] For the CORE run we initialize the model with ocean temperature, salinity, and phosphate from the World Ocean Atlas 2005 [Locarnini *et al.*, 2006; Antonov *et al.*, 2006; Garcia *et al.*, 2006] and alkalinity from Global Ocean Data Analysis Project (GLODAP) [Key *et al.*, 2004]. We initialize

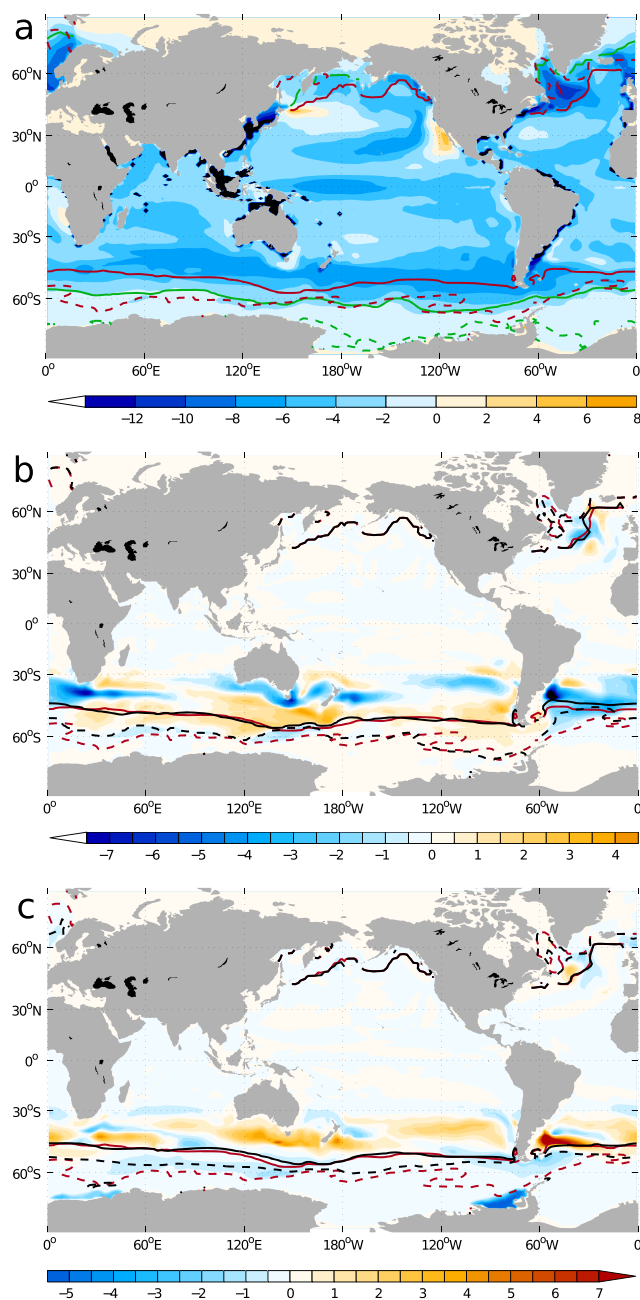


Figure 2. SST anomaly (in K; color code) and sea ice extent (lines) including all grid cells with at least 15% sea ice concentration in (a) LGM-CORE, (b) shift10N-LGM, and (c) shift10S-LGM. Maximum (closed lines) and minimum (broken lines) sea ice extent for CORE (green), LGM (red), and shifted wind scenarios (black).

the carbon cycle with preindustrial conditions calculating present-day minus anthropogenic DIC from GLODAP [Key *et al.*, 2004]. The physics in the CORE-1 data set describes more a present-day ocean. However, due to this carbon cycle initialization we consider the CORE run an approximation to the “preindustrial” state.

[13] For the LGM runs, we lowered the sea level by 116 m to account for the increased storage of water in land ice. Accordingly, we conserved the total inventory of salt, which led to an increase in ocean salinity by a constant

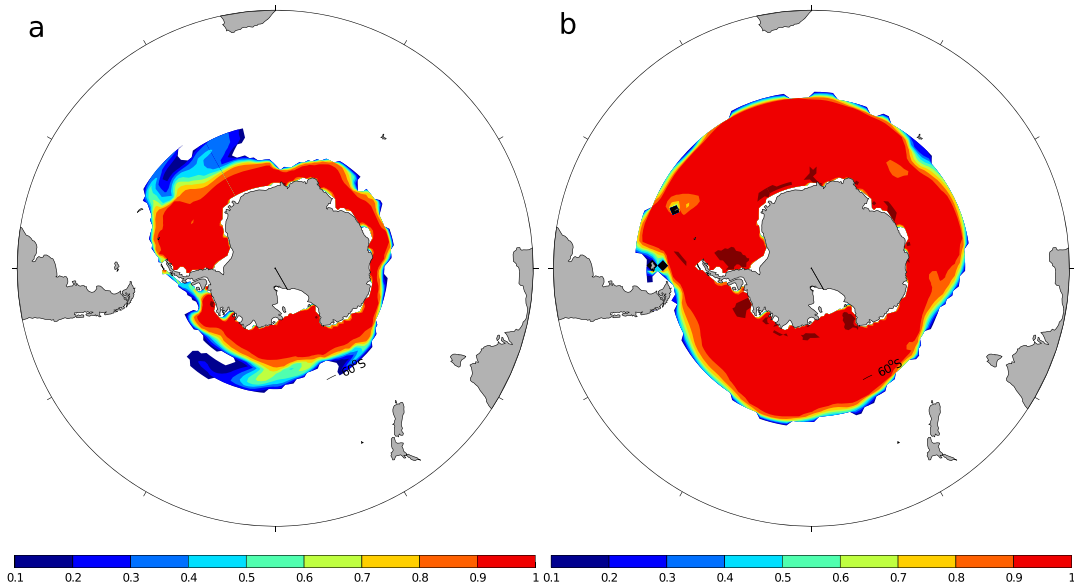


Figure 3. Fractional sea ice cover in the LGM run. (a) Minimum (March average) and (b) maximum (September average).

value of about 1 practical salinity unit (psu). Temperature, however, was initialized with present-day values, i.e., too warm, leaving it to the model to adjust to the glacial forcing. The simulations of the coupled atmosphere-ocean model COSMOS for LGM [Zhang *et al.*, 2013], from which we use ocean surface forcing fields, follow the protocol of the model intercomparison PMIP3 (available at <http://pmip3.lscce.ipsl.fr/>).

[14] Furthermore, at the LGM we multiplied the initial conditions of preindustrial concentrations of the conservative tracers (phosphate, silicate, alkalinity, and DIC) by a constant factor in order to conserve the total inventories in spite of the lower sea level. We also initialized the atmospheric partial pressure of carbon dioxide $p\text{CO}_2^{\text{atm}}$ to a preindustrial value of $280 \mu\text{atm}$ in all runs (thus keeping the total ocean-atmosphere carbon inventory constant between runs) and allowed it to vary freely through exchange with the ocean, thereafter.

[15] Model runs were started from rest and integrated forward in time for 5000 years, with the last 100 years used for detailed evaluation. As model runs were required to run for

several thousand model years, special care had to be taken such that the global inventory of alkalinity and phosphate remained conserved also over these long times. In order to achieve a satisfactory conservation especially of alkalinity over the long integration period that we used, we used the fully nonlinear free surface formulation provided by the MITgcm model [Campin *et al.*, 2004].

2.4. Scenarios: Shifting the Winds

[16] In a number of model sensitivity runs, the belt of strong westerly winds around Antarctica was then shifted by 5 or 10° northward or southward, leading altogether to six simulation scenarios (Table 1).

[17] We shifted both the zonal and meridional components of the wind, in order to shift also the net effect of the wind on the ocean through Ekman pumping. Resulting wind speed and wind stress for both CORE and LGM are found in Figure 1. For these experiments winds were mapped to a new latitude $\varphi' = \varphi + d\varphi$. The latitude shift $d\varphi(\varphi)$ is a piecewise linear function of latitude which is zero outside the range $-75^\circ < \varphi < -25^\circ$, increases linearly from zero to

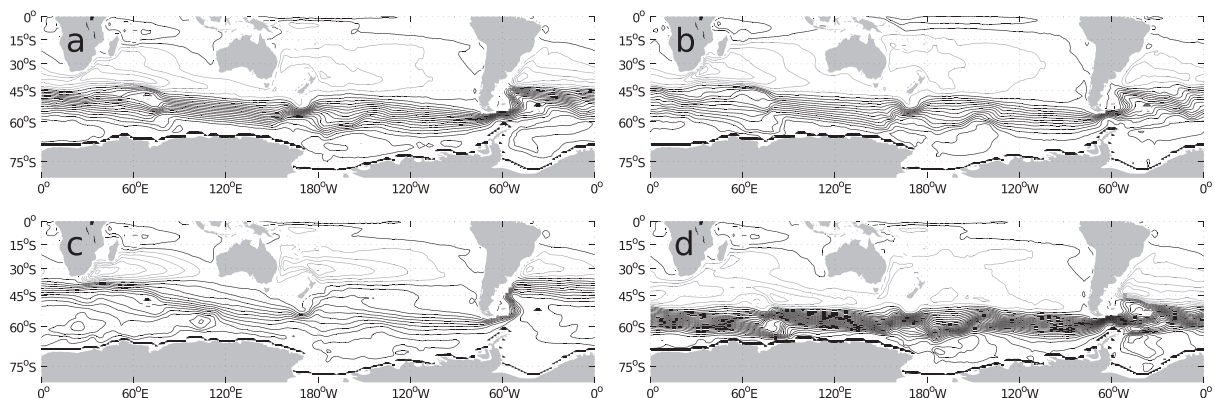


Figure 4. Southern Hemisphere horizontal stream function for (a) LGM, (b) CORE, (c) shift10N, and (d) shift10S. Isolines are drawn every 20 Sv; negative values are indicated by gray lines.

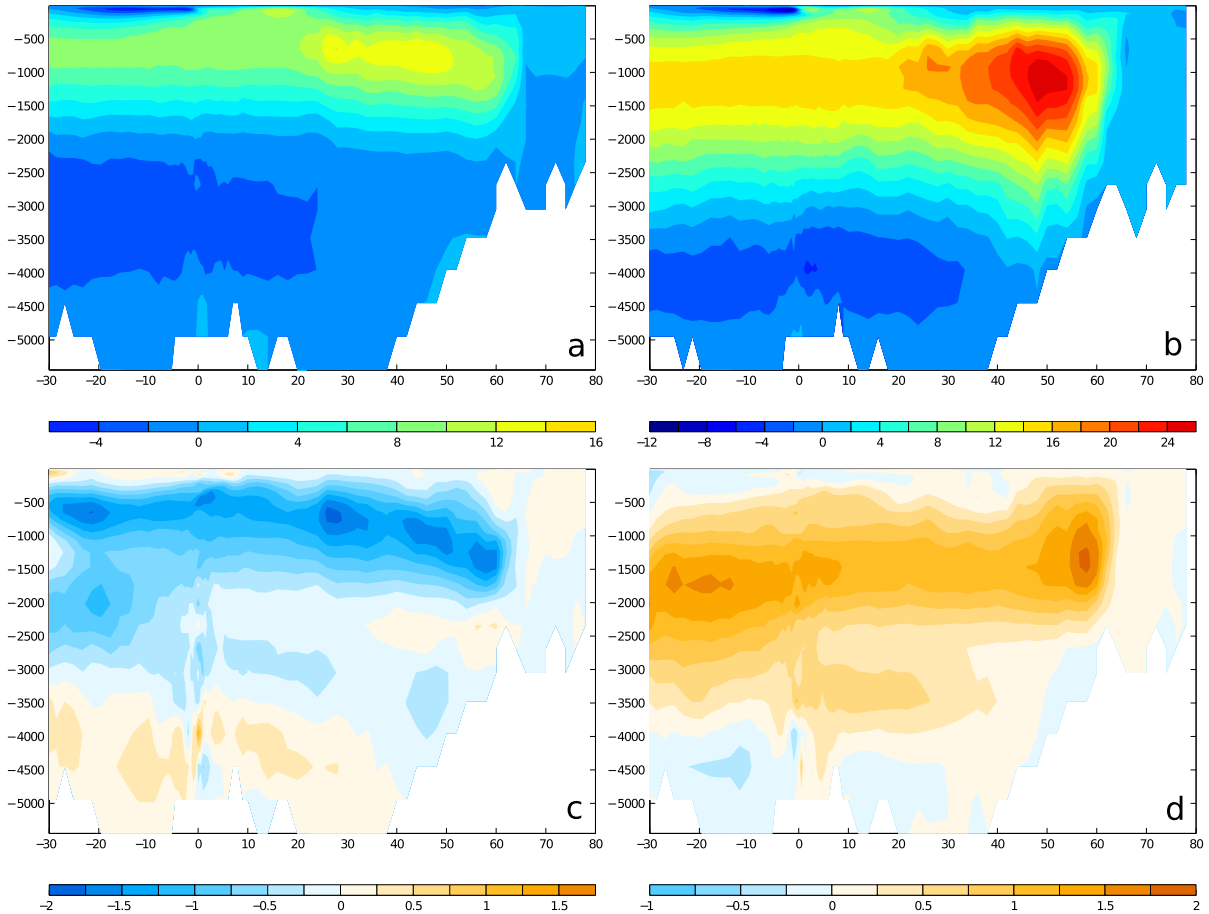


Figure 5. Overturning stream function in the Atlantic (Sv): (a) LGM and (b) CORE. Anomalies calculated as (c) shift10N-LGM and (d) shift10S-LGM.

its maximum value a for $-75^\circ < \varphi < -50^\circ$, and decreases linearly from a to zero for $-50^\circ < \varphi < -25^\circ$. The amplitude of the wind shift a was set to $a = \pm 5^\circ$ and $\pm 10^\circ$.

[18] A notable difference to others [Toggweiler *et al.*, 2006; d’Orgeville *et al.*, 2010], which became necessary by using a fully prognostic sea ice model, is that we did not shift the *wind stress*, but the *wind*. Because the wind enters the bulk wind stress formula nonlinearly, the effect on wind stresses is not only a shift in location of the maximum but also some change in amplitude. In ice-covered model boxes, the momentum transfer to the ocean is calculated as the weighted average of wind stress over the ice-free area and momentum transfer from drifting ice in the ice-covered area. This leads to a marked increase of the maximum momentum transfer for the southward shift, where the strongest winds often occur over ice (Figure 1b). Wind speed also affects turbulent fluxes of heat and fresh water, so our shifts in winds also affect these directly (and not only indirectly, through changing the ocean state).

3. Results

3.1. Glacial Ocean and Comparison to the Reference Run

[19] After an integration time of 5000 years the simulations have come close to an equilibrium; remaining

temperature and salinity trends are small ($< 60 \mu\text{K yr}^{-1}$ and $< 80 \mu\text{psu yr}^{-1}$). The LGM simulation has reached an average ocean temperature of 1.2 K, about 3.6 K lower than in the CORE simulation. This is in agreement with proxy data, which indicate an ocean cooling at the LGM of $-3.25 \pm 0.55 \text{ K}$ [Clark *et al.*, 2009] but a stronger cooling than in PMIP2 experiments [Murakami *et al.*, 2008], showing only a cooling of about 2 K. Global mean sea surface temperature (SST) is 3.8 K colder at the LGM than in the control run, which agrees with $-3.5 \pm 1.2 \text{ K}$ of the model-based interpretation of reconstructed LGM change in SST based on the MARGO data set [Annan and Hargreaves, 2013]. The dominant patterns of the SST anomaly at the LGM (pronounced cooling in the North Atlantic and around 50°S in the Southern Ocean) also agree with Annan and Hargreaves [2013] (Figure 2a). However, some small, localized features disagree, e.g., the warming our model generates in the North Pacific.

[20] The cooling of the ocean at LGM is accompanied by a large northward extension of the sea ice cover around Antarctica (Figure 3): The maximum sea ice-covered area is $39.2 \cdot 10^6 \text{ km}^2$, more than twice the area in the CORE simulation ($17.8 \cdot 10^6 \text{ km}^2$), and even in SH summer an area of $14.8 \cdot 10^6 \text{ km}^2$ remains ice covered, compared to only $0.6 \cdot 10^6 \text{ km}^2$ in the CORE simulation. Unlike most of the PMIP2 models, except HadCM [Roche *et al.*, 2012], our model thus produces a stronger seasonal cycle of sea ice area

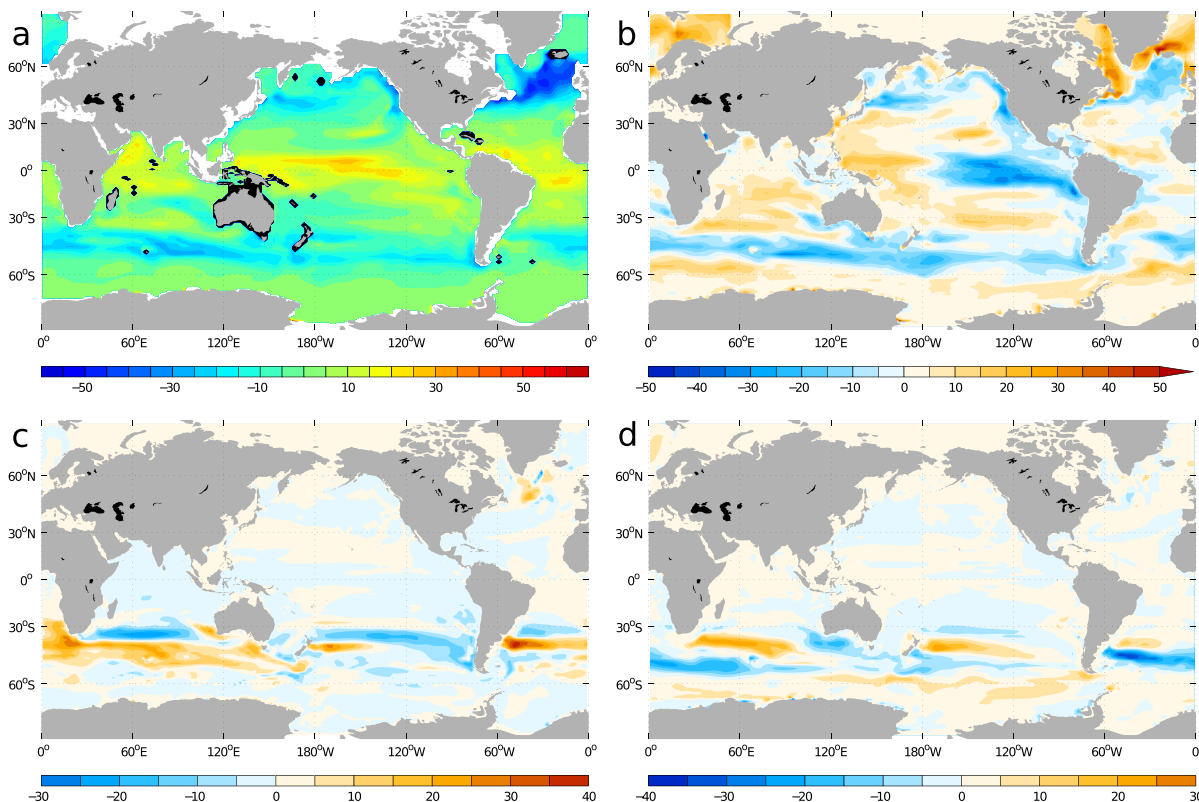


Figure 6. Sea-air gas exchange ($\text{g C m}^{-2} \text{ yr}^{-1}$, positive out of the ocean) in (a) the LGM model run and difference of this flux in (b) LGM-CORE, (c) shift10N-LGM, and (d) shift10S-LGM.

during the LGM than at present and matches quite well the maximum sea ice extent from proxy-based reconstructions [Gersonde *et al.*, 2005].

[21] The location of the SH maximum in zonal wind stress is shifted to the north by about 4° in the LGM forcing. The wind speed is also somewhat larger (7.9 m s^{-1} in the zonal mean at the location of the maximum versus 6.5 m s^{-1}) than in the CORE forcing. This and the changed density structure through sea ice formation [Gent *et al.*, 2001] lead to a slightly stronger Antarctic Circumpolar Current (ACC), with transport through Drake passage being 153 sverdrup (Sv), compared to 123 Sv in the CORE simulation and a somewhat weaker Weddell gyre (Figures 4a and 4b). Otto-Bliesner *et al.* [2006] has found a much stronger increase in ACC transport (from 195 to 320 Sv) in a coupled model run (Community Climate System Model (CCSM) version 3) that also includes a prognostic sea ice model. In CCSM4, however, the Drake passage through-flow changes only from 175 Sv to 231 Sv, when moving from a preindustrial to the LGM state [Brady *et al.*, 2013].

[22] In the model presented here, the AMOC in the LGM is weaker and shallower than in the CORE state (Figures 5a and 5b), with a maximum transport of 14.1 Sv (LGM) versus 25.7 Sv (CORE). In that as in many other aspects our LGM results mostly resembles the LGM state from the CCSM3 model presented in Otto-Bliesner *et al.* [2007]. Interestingly, the coupled model run from which the forcing data for this run was derived [Zhang *et al.*, 2013] has a slightly stronger AMOC at the LGM than in the preindustrial control, which is also the case for other simulations of the PMIP3 generation of coupled models [e.g., Brady *et al.*, 2013]. The

strength of the AMOC at the LGM is still difficult to evaluate, because of large uncertainties in the reconstructions [e.g., Lynch-Stieglitz *et al.*, 2007]. Our LGM AMOC is about 45% weaker and shallower than in the CORE run. This is in agreement with Hesse *et al.* [2011], who compared Atlantic $\delta^{13}\text{C}$ in reconstructions and simulations. Other studies, however, point toward a shallow but more vigorous glacial AMOC (e.g., Lippold *et al.* [2012], based on $^{231}\text{Pa}/^{230}\text{Th}$). While models nowadays are found to support a weaker [Hesse *et al.*, 2011], similar [Ritz *et al.*, 2013], or stronger [Zhang *et al.*, 2013; Brady *et al.*, 2013] LGM AMOC, the paleo reconstructions indicate that the uncertainties in the proxies data need to be reduced significantly to come to a final data-based conclusion [e.g., Lynch-Stieglitz *et al.*, 2007; Huybers *et al.*, 2007; Marchal and Curry, 2008; Burke *et al.*, 2011].

[23] The changes in ocean circulation and the induced changes in the ocean carbon cycle lead to a final atmospheric $p\text{CO}_2$ of $264 \mu\text{atm}$ in the LGM run, $40 \mu\text{atm}$ lower than in the CORE run. Processes that contribute to the lower $p\text{CO}_2$ in the LGM run are the lower SST and higher alkalinity, with some slight counteracting tendency through the higher average salinity. However, there is also a contribution from a changed vertical distribution of DIC in the ocean. Remember that a number of other processes potentially changing glacial $p\text{CO}_2$ were not considered here such as changes in iron cycling, and that our CORE run is forced with present-day, not with preindustrial, boundary conditions.

[24] The sea-air gas exchange of CO_2 shows an increase in ocean uptake of CO_2 throughout the midlatitude North Atlantic Ocean (Figures 6a and 6b), in addition to a decrease

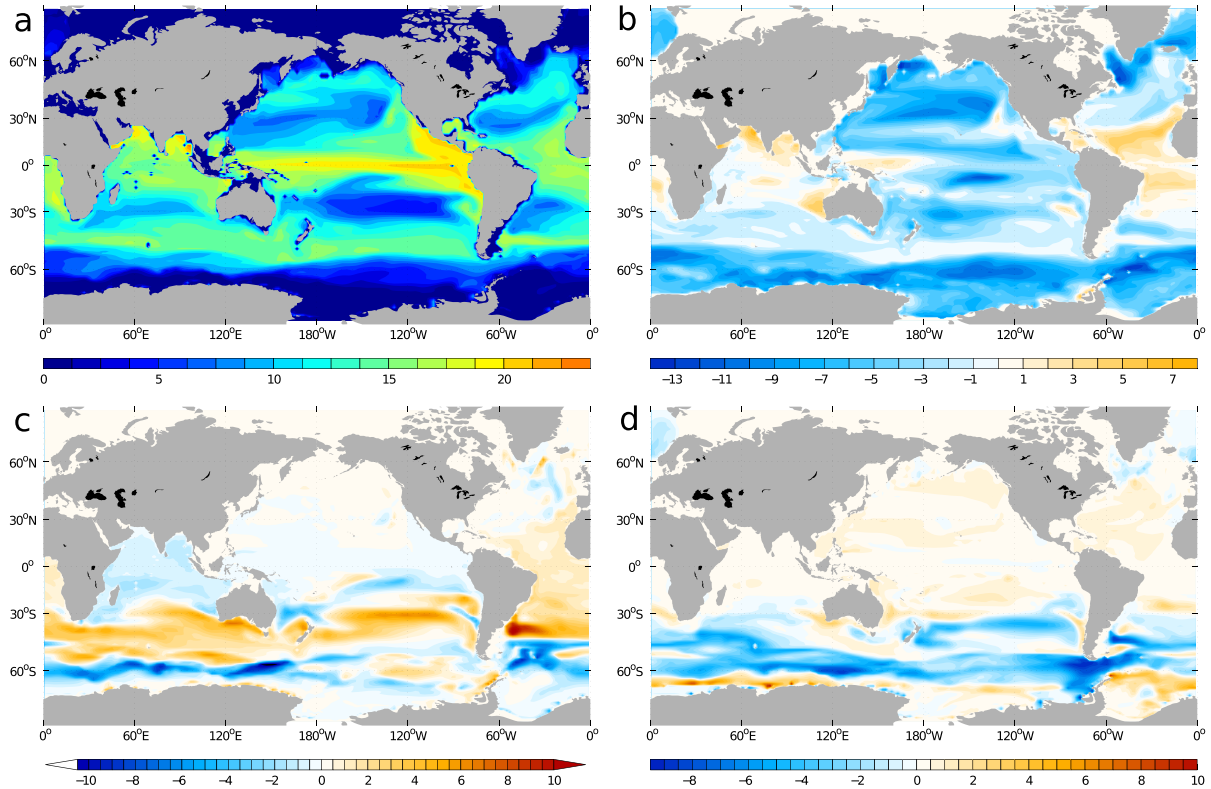


Figure 7. Vertical sinking flux of particulate organic carbon at 100 m depth ($\text{g C m}^{-2} \text{yr}^{-1}$) in (a) the LGM model run and difference of this flux in (b) LGM-CORE, (c) shift10N-LGM, and (d) shift10S-LGM.

in the biological pump (Figures 7a and 7b) at those latitudes. The increased uptake of CO₂ must therefore primarily be driven physically by an increase in the solubility, i.e., the physical pump, related to changed air-sea heat fluxes. Both the increased gas exchange and the decreased physical pump would lead to an increased advection of DIC with the North Atlantic Current into the seasonally ice-covered regions. These regions, which extend over most of the Irminger and Labrador Sea in the LGM run, thus show a strong supersaturation of CO₂ and outgassing, coinciding with a much reduced export production.

3.2. Effect of Changing Winds on the Physics

[25] The shift in the latitude of the westerly wind belt on the Southern Hemisphere leads to a pronounced change in the strength of the ACC in our glacial model setup. As shown in Figure 8b the transport through Drake passage increases under a southward shift and decreases under a northward shift, with most of the change already occurring for a $\pm 5^\circ$ shift. This change in strength is accompanied by some change in the mean path of the ACC (Figures 4c and 4d) with the position of the ACC in the Atlantic and Indian Oceans moving north (south) under a northward (southward) wind shift. In the Pacific Ocean, this shift is less pronounced, because the ACC is rather tightly constrained here by interaction with topography [Olbers *et al.*, 2004], namely the Macquarie Ridge and the topographical obstacles around Drake passage.

[26] The shift in the position of the ACC at the longitude of South Africa has implications to the degree to which the subtropical gyres in the South Atlantic and Indian are

connected to a supergyre, i.e., for the Agulhas leakage as it is represented in coarse-resolution circulation models. This will be discussed further below.

[27] The change in the strength of the ACC can be traced back directly to the applied wind stress: *Gent et al.* [2001] have shown in a coarse-resolution model setup similar to ours that the main factor for the strength of the ACC is the northward Ekman transport at the location of Drake passage. The Ekman transport at the latitude of the tip of South America, calculated from the wind stress shown in Figure 1, covaries strongly with the ACC transport through Drake passage (Figures 8b and 8d).

[28] A second major circulation change is an increase of the strength of the AMOC under a southward shift and a decrease under a northward shift (Figure 8a). Again, the largest part of the change already occurs for a 5° shift, with some saturation occurring for larger shifts. The relative magnitude of the change, however, is much smaller for the AMOC ($\pm 10\%$) than for the ACC ($\pm 50\%$) transport. The change in AMOC strength is not accompanied by a strong change in the pattern of the AMOC circulation, however (Figures 5c and 5d), especially that the depth of the Glacial North Atlantic Deep Water (GNADW) circulation cell remains almost unchanged.

[29] *Sijp and England* [2008, 2009] have found a qualitatively similar reaction of the AMOC strength to shifts in SH westerlies in their model runs for a preindustrial climate. In their case, the change in AMOC strength was related to a change in the warm-water exchange, the so-called Agulhas leakage, between the Indian and Atlantic Oceans: The position changes of the ACC south of Africa affect

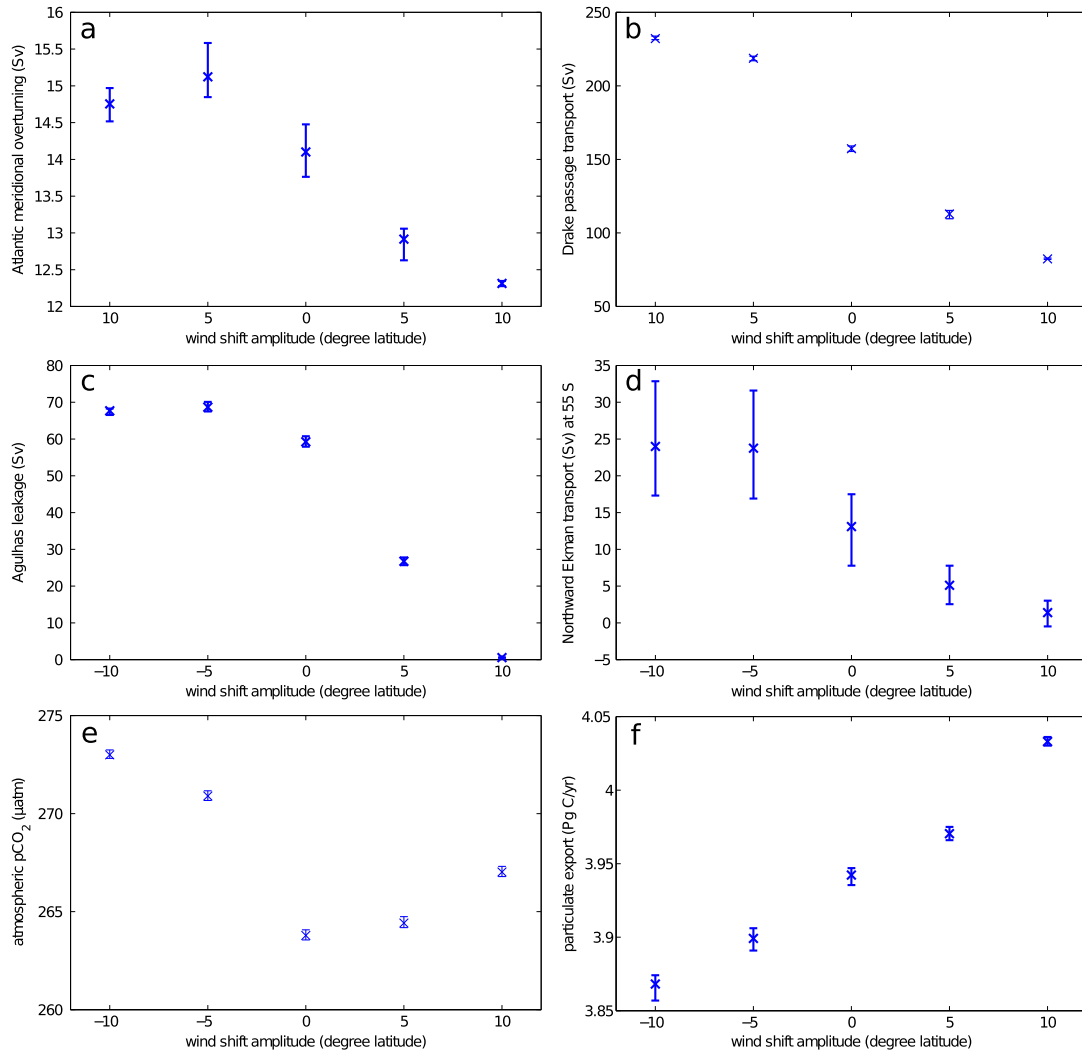


Figure 8. Dependency of some important integral quantities on the amplitude of the wind shift (negative = southward). (a) Atlantic meridional overturning. (b) Drake passage transport. (c) Agulhas leakage. (d) Northward Ekman transport at the latitude of the tip of South America. (e) Atmospheric $p\text{CO}_2$. (f) Global export production of organic matter at 100 m depth. Crosses indicate mean values over the last 100 years; vertical bars are the maximum and minimum values attained during that time span, i.e., an indicator of variability, not an error bar.

this exchange and by this, also the salinity balance of the Atlantic basin. In our model runs we see a similar pattern in the Agulhas strength, which we defined as the strength of the exchange (in Sverdrup) of the two subtropical gyres in the South Indian and Atlantic Ocean basins (Figure 8c). This exchange decreases toward zero for a northward shift in the winds, because the path of the ACC approaches the African continent.

[30] In spite of this similarity we argue that our mechanism for the change in AMOC strength is quite different from that seen for a preindustrial background state in *Sijp and England* [2008, 2009]: the mechanism by which the Agulhas leakage affected their AMOC strength was by a change in the intermediate water salinity in the South Atlantic. A stronger Agulhas leakage led to an increased influx of relatively warm and salty water into the South Atlantic. While the excess heat was then lost to the atmosphere during the northward movement of this water mass,

the excess salinity remained and increased the salinity in the North Atlantic, leading to increased overturning and a stronger AMOC.

[31] In our case, however, the increase in Agulhas leakage with a southward shift of the westerlies is accompanied by a *decrease*, not an increase in intermediate water salinity and vice versa (Figure 9). This is due to the fact that when the leakage increases, the northward Ekman transport at the tip of South America also increases (Figure 8d), increasing the northward transport of relatively fresh water masses and the formation rate of fresh and cold Antarctic Intermediate Water (AAIW) and Subantarctic Mode Water (SAMW).

[32] From the salinity balance alone one would thus expect a decrease of the AMOC with a southward shift of the westerlies, which is opposite to what we find. The decreased salinity, however, is also accompanied by a decrease in temperature (Figure 10b), partly offsetting the effect on

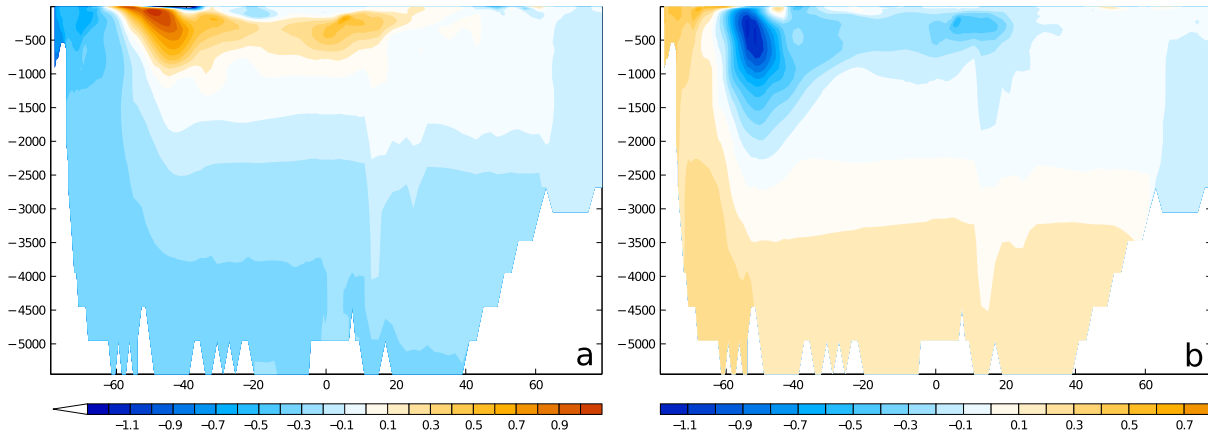


Figure 9. Change in the zonally averaged salinity (psu) within the Atlantic basin (cut off at 30°E and 30°W in the South Atlantic): (a) shift10N-LGM and (b) shift10S-LGM.

density. But more important, the increased northward Ekman transport implies also a strong increase in Southern Ocean upwelling. In our case the changed AMOC thus seems to be more pulled by upwelling in the south than pushed by downwelling in the north, i.e., driven more by changes in the upwelling of circumpolar deep water (CDW) and less by GNADW formation. The important role of the Southern Ocean upwelling is also seen in the temperature changes (Figures 10a and 10b): Stronger Ekman transport and thus stronger Southern Ocean upwelling and intermediate water mass formation lead to a colder ocean, with the largest cooling in the AAIW (and vice versa).

3.3. Effect of Changing Winds on the Carbon Cycle

[33] Unlike hypothesized by *Toggweiler et al.* [2006], but consistent with a number of recent modeling studies that—starting from a modern or preindustrial climate—shift the SH wind belt [*Tschumi et al.*, 2008; *Menviel et al.*, 2008; *d’Orgeville et al.*, 2010], we find only a weak sensitivity of atmospheric $p\text{CO}_2$ to the position of the SH westerlies in a glacial climate. In fact, both the northward and the southward shifts lead to a weak increase in atmospheric $p\text{CO}_2$, by 3 μatm for a 10° northward shift and by 9 μatm for a 10° southward shift (Figure 8e).

[34] A condensed view of the most important changes in both the ocean physics and the carbon cycle is presented in Figure 11. Here it becomes apparent that the complex interplay of changes in the biological and physical pump have to be analyzed together to understand the simulated pattern of rises in atmospheric CO₂ in both a northward and southward shift of the SH westerly wind belt.

[35] In the following the results are described in detail. The most important changes are restricted to the SH. For reasons of simplicity, whenever we refer to an area north of a specific latitude this implies the part of the SH north of that latitude even if this is not explicitly mentioned.

3.3.1. A Northward Shift of the Westerly Winds

[36] During a northward shift of the wind the upwelling zone is broadened. As a result, CO₂ outgassing is enhanced in the Southern Ocean. The increased upwelling of nutrient-rich waters also enhances export production in the Southern Ocean. The carbon outgassing is stronger than the drag of CO₂ into the ocean following the enhanced export production, and therefore, a small net atmospheric CO₂ increase is simulated (Figure 11b).

[37] In detail (scenario shift10N), DIC in surface and intermediate waters above 1500 m is increased north of 60°S but decreased further south and in deep waters (Figure 12a).

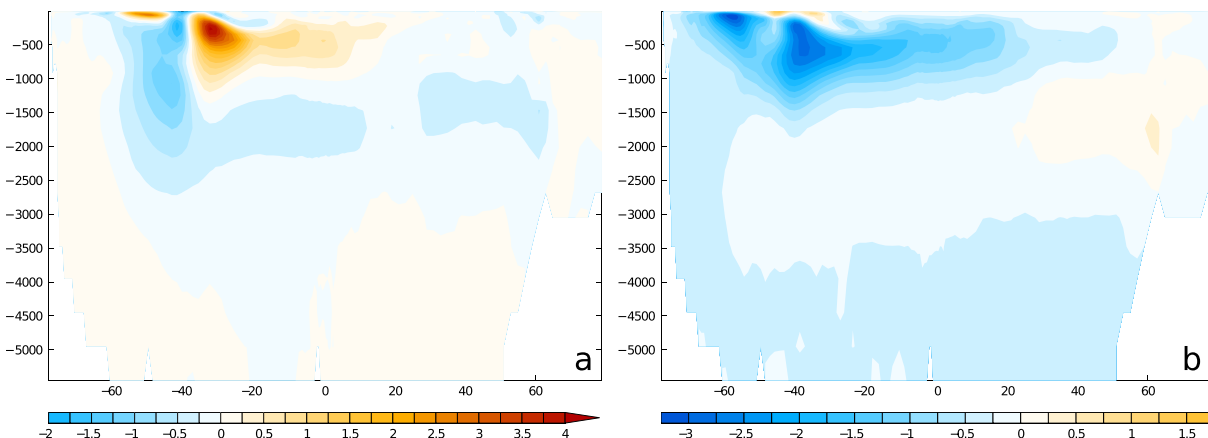


Figure 10. Difference in zonally averaged potential temperature Θ (K) in (a) shift10N-LGM and (b) shift10S-LGM.

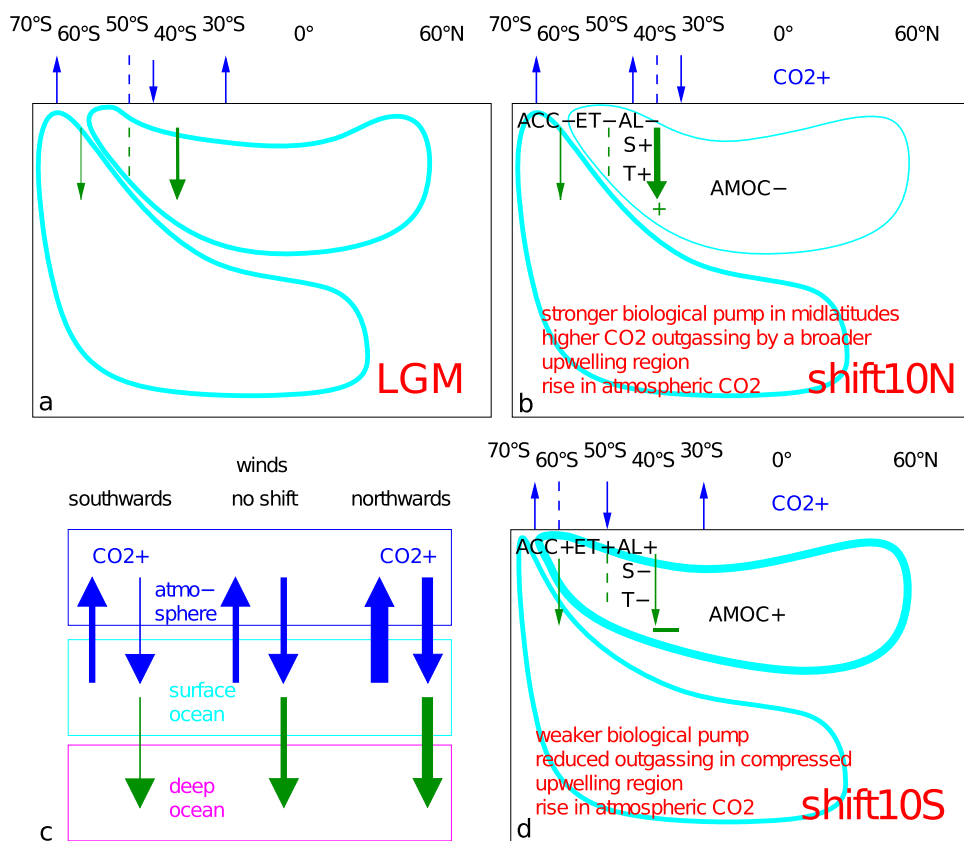


Figure 11. Conceptual view of how changes in the SH winds influence the ocean circulation and the carbon cycle. States for (a) LGM, (b) shift10N, and (d) shift10S as function of latitude and depth. (c) Condensed changes in the carbon cycle comparing the LGM simulations. Strength of the biological pump (green) and of the gas exchange (blue) depict how carbon varies between atmosphere, surface, and deep ocean. ACC: Antarctic Circumpolar Current, ET: Ekman transport, and AL: Agulhas leakage.

These anomaly patterns correspond to increased DIC in AAIW and SAMW but decreased DIC in Antarctic bottom water (AABW). The wind-induced changes in the vertical distribution of DIC are very similar to the changes in salinity (Figures 9a and 12a). Changes in PO_4^{3-} are somewhat more complicated. A dominant rise in PO_4^{3-} is found above 2000 m water depth between 60 and 40°S in line with the rise in DIC there, but PO_4^{3-} concentration in surface and intermediate waters drop between 40°S and the equator and are therefore decoupled from both anomalies in DIC and salinity (Figure 12c). This suggests that north of 40°S, variations in the carbon pumps have different impacts on the carbon cycle than south of 40°S. A similar decoupling was detected for the present day at 30°S, dubbed the Southern Ocean biogeochemical divide [Marinov *et al.*, 2006].

[38] This picture of decoupled carbon pumps is also supported by a closer look into gas exchange and export production rates. South of 40°S CO_2 outgassing is enhanced, while north of it, the ocean takes up CO_2 (Figure 6c). This pattern is especially seen in the Indian and Atlantic Oceans, but only to a small extent in the Pacific Ocean. Export production of organic matter to the deep ocean, on the other hand, is changed throughout the Southern Ocean without a distinct transition around 40°S (Figure 7c). We found a band of decreased export around 60°S and increased export 30–50°S.

[39] Around 40°S AAIW and SAMW subduct again, which make an increased outgassing north of it due to enhanced upwelling of carbon-rich deep waters impossible. On the contrary, CO_2 uptake of the ocean via gas exchange is increased north of 40°S. The distinct decoupling of DIC and PO_4^{3-} north of 40°S is therefore caused by this additional oceanic carbon uptake. Increased concentrations of DIC in the surface water masses lead also to higher DIC in waters which penetrate also north of the equator (Figure 12a).

[40] The northward wind shift also leads to a northward displacement of the summer sea ice extent (Figure 2b). In the Atlantic Ocean also winter sea ice is shifted north by a few degrees. Here SST dropped locally by more than 5 K in an area where outgassing of CO_2 to the atmosphere is largest (Figure 6c). In the Indian section of the Southern Ocean, another region with enhanced outgassing of CO_2 , SST at the sea ice edge increases by 1 to 3 K. This illustrates that the interplay of various processes (SST, sea ice cover, and carbon content of the upwelling waters) define whether the changes in local gas exchange is directed into or out of the ocean.

3.3.2. A Southward Shift of the Westerly Winds

[41] On the contrary, when the westerly winds are shifted southward, the upwelling zone in the Southern Ocean is contracted. This reduces the amount of upwelling nutrients that travel north via AAIW and SAMW, thus weakening the biological pump in the subpolar region. Total outgassing of

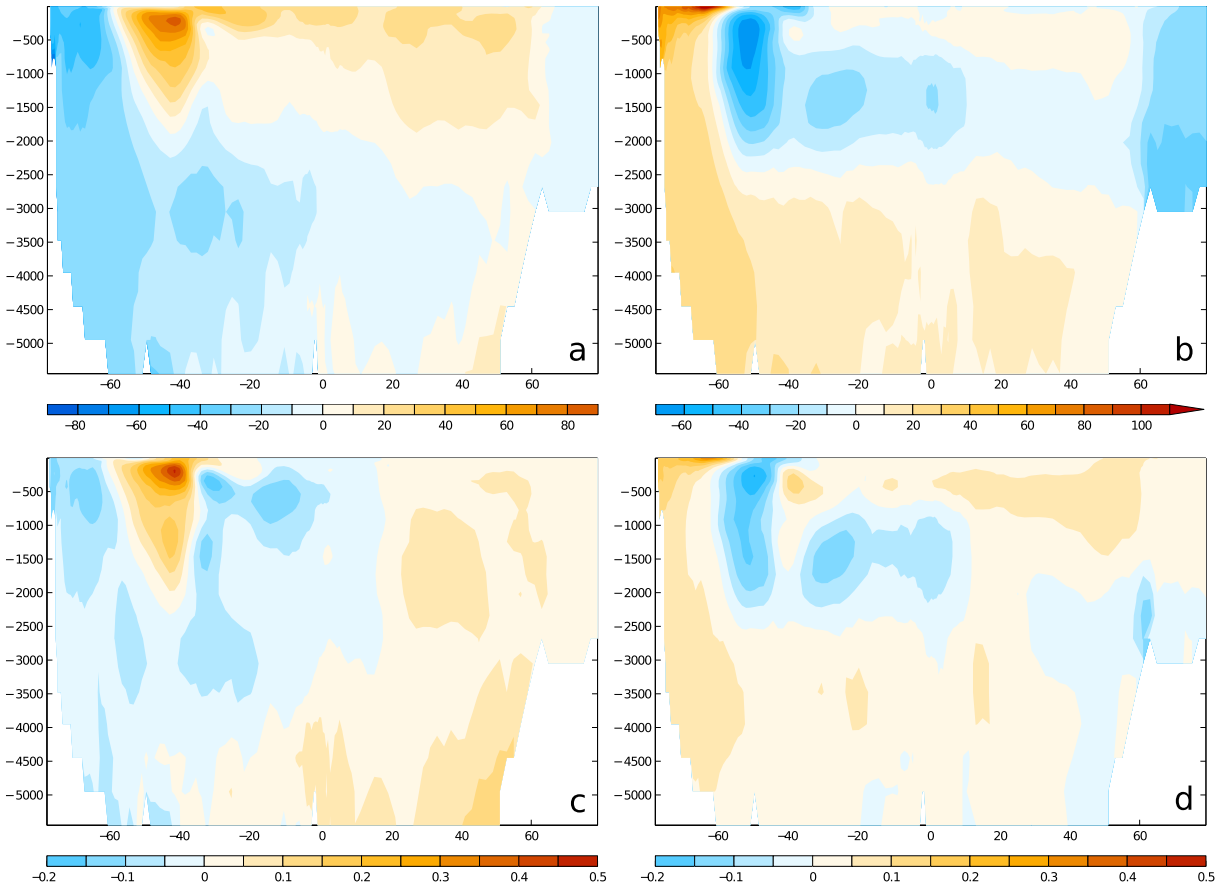


Figure 12. Zonally averaged (a, b) DIC concentration (mmol m^{-3}), (c, d) phosphate concentration (mmol m^{-3}) in (a, c) shift10N-LGM and (b, d) shift10S-LGM.

CO₂ is changed only slightly, but the reduced biological productivity further north reduces the oceanic carbon uptake, leading again to a rise in atmospheric CO₂ (Figure 11d).

[42] The details of scenario shift10S are as follows: Intermediate waters above 2000 m water depth north of 60°S and surface waters in the band 60–30°S are decreased in DIC and PO₄³⁻; waters further south or deeper (consisting of circumpolar deep water) are enriched (Figures 12b and 12d). This time, both variables are not decoupled to the north, but again, patterns of changes are similar to those in salinity (Figure 9b).

[43] We find a clearly reduced export production throughout 60–30°S (Figure 7d) which is directly explained by the reduced nutrient concentration in surface waters north of 60°S. This leads to the overall picture that the global export production of organic matter decreases with southward shifted winds and increases with northward shifted winds (Figure 8f).

[44] Patterns in gas exchange rate are very patchy and nearly opposite to those found for the northward shifted winds (Figure 6d). Around 60°S we found that CO₂ outgassing between 50–40°S exists in a band with oceanic CO₂ uptake. Some more outgassing patches in the Indian and Pacific Oceans are seen around 40°S. For the southward shift in the westerly wind the latitude of 40°S does not seem to act as a clear divide between different effects north and south of this latitude.

[45] If wind is shifted southward, winter sea ice extent is nearly unchanged, but summer sea ice is shifted north probably due to enhanced heat loss to the atmosphere (Figure 2c). The contraction and southward displacement of the upwelling zone lead to rising SST north of that area throughout the Southern Ocean with largest warming of more than 5 K in the Atlantic sector. Throughout most of the Southern Ocean (apart from an area in the Indian Ocean southwest of Africa) we find a warming ocean surface, but CO₂ uptake from the atmosphere (Figures 2c and 6d), again illustrating that various processes need to be considered together for an understanding of carbon cycle changes.

4. Discussion

[46] The hypothesis of *Toggweiler et al.* [2006] on the impact of changes in Southern Ocean westerlies on paleoclimate and the carbon cycle was taken up frequently in the interpretation of new paleo records covering the LGM or Termination I [e.g., *Anderson et al.*, 2009]. However, there is no clear evidence from paleo data or climate models that such a change in the westerly wind belt even occurred, and it is unclear that the response of the carbon cycle, and especially the deglacial rise in atmospheric CO₂, can be connected with such changes.

[47] In a recent review *Kohfeld et al.* [2013] compiled all available paleo data on LGM wind shifts. The data show no

clear evidence for one specific change in the SH westerly winds at the LGM. Although a strengthening or an equatorward displacement of the westerlies at the LGM are at most in line with the paleo data, the opposite cannot be ruled out either. The proxy data contained in that review can be distinguished by the kind of evidence they provide (moisture, dust, SST, marine productivity, frontal shifts, Agulhas leakage, deep water isolation) from which final changes in wind were deduced. The most common data-based evidence for a large equatorward shift in the westerly wind belt at the LGM are provided by suggested changes in moisture based on pollen assemblages, lake level status, glacial moraines, and accumulation rates in ice cores. However, none of the PMIP2 models that produce realistic changes in precipitation at the LGM show such a large equatorward shift in the westerlies [Rojas *et al.*, 2009]. Even further, HadAM3, an atmospheric GCM which simulates the evidences for moisture changes at the LGM obtained from proxy data best, shows a strengthening of the westerlies by 1 m s^{-1} and a poleward shift by 2° [Sime *et al.*, 2013]. While the proxy-based evidence of Kohfeld *et al.* [2013] allows an interpretation of an equatorward shift in the westerlies by $3\text{--}15^\circ$, the simulations of Sime *et al.* [2013], which are otherwise in good agreement with the evidences for LGM moisture changes, prefer a poleward shift but also allow an equatorward displacement of the westerlies by no more than 3° . In a different study using an atmospheric GCM, Lee *et al.* [2011] showed that a Northern Hemispheric cooling might lead to a southward shift of the intertropical convergence zone, but not necessarily to a southward shift of the SH westerlies, probably more to their strengthening.

[48] According to the Toggweiler hypothesis, the westerly winds shifted equatorward at the LGM would move poleward again at the beginning of the deglaciation, leading to enhanced upwelling of old and carbon-rich water in the Southern Ocean which might then explain the atmospheric CO₂ rise. Anderson *et al.* [2009] suggested that such an enhanced upwelling would also enhance AAIW and SAMW. We indeed find enhanced AAIW and SAMW for southward shifted SH westerlies in our model giving some support for the connection of westerly winds and the northward moving intermediate water masses.

[49] Our study focused on the analysis of the SH westerly wind hypothesis on ocean physics and on the carbon cycle based on a more sophisticated setup than previously performed. We generated a LGM background state, which is in reasonable agreement with available reconstructions and which leads to a response of the AMOC to the wind shifts which is similar to responses in other models applied for modern background conditions, but for a different reason. We do not intend to propose a LGM model configuration which can explain the full spectrum of carbon cycle observations, e.g., the atmospheric $p\text{CO}_2$ reduction of about $80\text{--}100 \mu\text{atm}$ and corresponding changes in carbon isotopes [Schmitt *et al.*, 2012; Matsumoto and Yokoyama, 2013]. Therefore, our LGM state shows only a reduction of atmospheric $p\text{CO}_2$ by $40 \mu\text{atm}$ mainly caused by ocean cooling and changed vertical distribution of DIC within the ocean. Important processes proposed by others for the explanation of the missing $p\text{CO}_2$ reduction are simply not contained in our modeling setup, e.g., (to name some recent ones) brine rejection changing Southern Ocean overturning fluxes, iron

fertilization, changes in nutrient utilization, shallow water carbonate sedimentation, weathering, rain ratio, deepening of particulate organic matter remineralization, a larger terrestrial carbon content, and carbonate compensation [e.g., Brovkin *et al.*, 2007; Bouttes *et al.*, 2011; Ciais *et al.*, 2012; Menviel *et al.*, 2012].

[50] A consequence of the fact that our model does not reproduce the LGM carbon cycle perfectly (with only about 50% of the change in atmospheric $p\text{CO}_2$ as seen in the data) is that the response of the carbon cycle in our simulations to the shifted wind experiments might also be underestimated. However, our analysis has already shown that the response of the system is highly nonlinear, with competing effects of physical and biological carbon pumps. It is therefore not possible to estimate which effect would be gained with a model, in which the carbon cycle fully agrees with reconstructions. Future simulation studies would be necessary here.

[51] A so far unsettled question is whether eddies, through their role in the Southern Ocean in vertical transport of momentum and lateral transport of heat and tracers, may reduce the sensitivity of the mean circulation to changes in wind stress, phenomena called eddy saturation and eddy compensation [e.g., Munday *et al.*, 2012]. The extent of eddy compensation and thus the sensitivity of the MOC to the wind depends on the surface boundary conditions [Hallberg and Gnanadesikan, 2006; Abernathey *et al.*, 2011], and models partially disagree on its size [e.g. Meredith and Hogg, 2006; Treguier *et al.*, 2010]. Studies that focus on the effect of changed winds on the carbon cycle require long integration times, making explicit resolution of eddies costly. Our model, like those of d'Orgeville *et al.* [2010], Tschumi *et al.* [2008], and Menviel *et al.* [2008], does not resolve eddies but uses the Gent-McWilliams parametrization [Gent *et al.*, 1995] to model their effect on the large scale flow. Whether this allows to model eddy compensation realistically is still an open question. Note, however, that the reaction of Southern Ocean carbon fluxes to the Southern Annular Mode is very similar in the eddy-resolving study of Dufour *et al.* [2013] and in the study of Hauck *et al.* [2013], which parameterizes eddies the same way as we do.

[52] According to our results, the impact of changes in the SH westerlies on ocean circulation and on atmospheric CO₂ during the deglaciation might have been as follows: Independent estimates [Kohfeld *et al.*, 2013] suggest that the SH westerly wind belt was probably shifted to the north by no more than 5° in the LGM. In the atmospheric forcing of our LGM simulation the maximum in zonal wind stress was already shifted north by 4° . We therefore argue that starting from our LGM reference simulation, a southward shift of the westerly winds by 5° (our experiment shift5S) is the closest analog to what might have happened in the past during Termination I. These changes in the SH winds probably evolved slowly over the whole deglaciation, not abrupt in a short time window of a few centuries. It might thus explain only a small part of less than 10% of the deglacial AMOC enhancement and a rise in atmospheric CO₂ by $7 \mu\text{atm}$ (our response in shift5S). Thus, it becomes clear that SH westerly wind belt variation was not the dominant process which tightly couples atmospheric CO₂ and high-latitude SH temperature during terminations or even whole glacial cycles.

[53] **Acknowledgments.** LGM forcing data were kindly provided by Xu Zhang. P.K. acknowledges support by the German Research Foundation DFG (project number KO 2937/5-1) and C.V. by the EU FP7 project CarboChange (grant agreement 264879). We thank Karen Kohfeld and two anonymous reviewers for their constructive suggestions on how to improve the article.

References

- Abernathy, R., J. Marshall, and D. Ferreira (2011), The dependence of Southern Ocean Meridional overturning on wind stress, *J. Phys. Oceanogr.*, *41*, 2261–2278, doi:10.1175/JPO-D-11-023.1.
- Ahn, J., and E. J. Brook (2008), Atmospheric CO₂ and climate on millennial time scales during the last glacial period, *Science*, *322*, 83–85, doi:10.1126/science.1160832.
- Anderson, R. F., S. Ali, L. I. Bradmilller, S. H. H. Nielsen, M. Q. Fleisher, B. E. Anderson, and L. H. Burckle (2009), Wind-driven upwelling in the Southern Ocean and the deglacial rise in atmospheric CO₂, *Science*, *323*, 1443–1448, doi:10.1126/science.1167441.
- Annan, J. D., and J. C. Hargreaves (2013), A new global reconstruction of temperature changes at the Last Glacial Maximum, *Clim. Past*, *9*(1), 367–376, doi:10.5194/cp-9-367-2013.
- Antonov, J., R. Locarnini, T. Boyer, A. Mishonov, and H. Garcia (2006), *World Ocean Atlas 2006 Volume 2: Salinity*, 182 p. S. Levitus (ed), NOAA Atlas NESDIS 62, U.S. Gov. Printing Office, Washington, D. C.
- Bouttes, N., D. Paillard, D. M. Roche, V. Brovkin, and L. Bopp (2011), Last Glacial Maximum CO₂ and $\delta^{13}\text{C}$ successfully reconciled, *Geophys. Res. Lett.*, *38*, L02705, doi:10.1029/2010GL044499.
- Brady, E. C., B. L. Otto-Bliessner, J. E. Kay, and N. Rosenbloom (2013), Sensitivity to glacial forcing in the CCSM4, *J. Clim.*, *26*(6), 1901–1925, doi:10.1175/JCLI-D-11-00416.1.
- Brovkin, V., A. Ganopolski, D. Archer, and S. Rahmstorf (2007), Lowering of glacial atmospheric CO₂ in response to changes in oceanic circulation and marine biogeochemistry, *Paleoceanography*, *22*, PA4202, doi:10.1029/2006PA001380.
- Burke, A., O. Marchal, L. I. Bradtmiller, J. F. McManus, and R. François (2011), Application of an inverse method to interpret ²³¹Pa/²³⁰Th observations from marine sediments, *Paleoceanography*, *26*, PA1212, doi:10.1029/2010PA002022.
- Campin, J.-M., and H. Goosse (1999), Parameterization of density-driven downsloping flow for a coarse-resolution ocean model in z-coordinate, *Tellus A*, *51*(3), 412–430, doi:10.1034/j.1600-0870.1999.t013-00006.x.
- Campin, J.-M., A. Adcroft, C. Hill, and J. Marshall (2004), Conservation of properties in a free-surface model, *Ocean Modell.*, *6*, 221–244, doi:10.1016/S1463-5003(03)00009-X.
- Ciais, P., et al. (2012), Large inert carbon pool in the terrestrial biosphere during the Last Glacial Maximum, *Nat. Geosci.*, *5*, 74–79, doi:10.1038/ngeo1324.
- Clark, P. U., A. S. Dyke, J. D. Shakun, A. E. Carlson, J. Clark, B. Wohlfarth, J. X. Mitrovica, S. W. Hostetler, and A. M. McCabe (2009), The Last Glacial Maximum, *Science*, *325*, 710–714, doi:10.1126/science.1172873.
- Delworth, T. L., and F. Zeng (2008), Simulated impact of altered Southern Hemisphere winds on the Atlantic Meridional Overturning Circulation, *Geophys. Res. Lett.*, *35*, L20708, doi:10.1029/2008GL035166.
- d’Orgeville, M., W. P. Sijp, M. H. England, and K. J. Meissner (2010), On the control of glacial-interglacial atmospheric CO₂ variations by the Southern Hemisphere westerlies, *Geophys. Res. Lett.*, *37*, L21703, doi:10.1029/2010GL045261.
- Dufour, C. O., J. Le Sommer, M. Gehlen, J. C. Orr, J.-M. Molines, J. Simeon, and B. Barnier (2013), Eddy compensation and controls of the enhanced sea-to-air CO₂ flux during positive phases of the Southern Annular Mode, *Global Biogeochem. Cycles*, *27*, 950–961, doi:10.1002/gbc.20090.
- Fischer, H., et al. (2010), The role of Southern Ocean processes on orbital and millennial CO₂ variations: A synthesis, *Quat. Sci. Rev.*, *29*, 193–205, doi:10.1016/j.quascirev.2009.06.007.
- Garcia, H., R. Locarnini, T. Boyer, and J. Antonov (2006), *World Ocean Atlas 2005, Volume 4: Nutrients (Phosphate, Nitrate, Silicate)*, 396 p., S. Levitus (ed), NOAA Atlas NESDIS 64, U.S. Government Printing Office, Washington, D. C.
- Gent, P. R., J. Willebrand, T. J. McDougall, and J. C. McWilliams (1995), Parameterizing eddy-induced tracer transports in ocean circulation models, *J. Phys. Oceanogr.*, *25*, 463–474.
- Gent, P. R., W. G. Large, and F. O. Bryan (2001), What sets the mean transport through Drake Passage?, *J. Geophys. Res.*, *106*(C2), 2693–2712, doi:10.1029/2000JC900036.
- Gersonde, R., X. Crosta, A. Abelmann, and L. Armand (2005), Seawater temperature and sea ice distribution of the Southern Ocean at the EPILOG Last Glacial Maximum: A circum-Antarctic view based on siliceous microfossil records, *Quat. Sci. Rev.*, *24*, 869–896, doi:10.1016/j.quascirev.2004.07.015.
- Gruber, N., et al. (2009), Oceanic sources, sinks, and transport of atmospheric CO₂, *Global Biogeochem. Cycles*, *23*, GB1005, doi:10.1029/2008GB003349.
- Hallberg, R., and A. Gnanadesikan (2006), The role of Eddies in determining the structure and response of the wind-driven Southern Hemisphere overturning: Results from the modeling Eddies in the Southern Ocean (MESO) project, *J. Phys. Oceanogr.*, *36*, 2232–2252, doi:10.1175/JPO2980.1.
- Hauck, J., C. Völker, T. Wang, M. Hoppema, M. Losch, and D. A. Wolf-Gladrow (2013), Seasonally different carbon flux changes in the Southern Ocean in response to the Southern Annular Mode, *Global Biogeochem. Cycles*, doi:10.1002/2013GB004600, in press.
- Hesse, T., M. Butzin, T. Bickert, and G. Lohmann (2011), A model-data comparison of $\delta^{13}\text{C}$ in the glacial Atlantic Ocean, *Paleoceanography*, *26*, PA3220, doi:10.1029/2010PA002085.
- Huybers, P., G. Gebbie, and O. Marchal (2007), Can paleoceanographic tracers constrain meridional circulation rates?, *J. Phys. Oceanogr.*, *37*, 394–407, doi:10.1175/JPO3018.1.
- Key, R. M., A. Kozyr, C. L. Sabine, K. Lee, R. Wanninkhof, J. L. Bullister, R. A. Feely, F. J. Millero, C. Mordy, and T.-H. Peng (2004), A global ocean carbon climatology: Results from Global Data Analysis Project (GLODAP), *Global Biogeochem. Cycles*, *18*, GB4031, doi:10.1029/2004GB002247.
- Kohfeld, K. E., R. M. Graham, A. M. de Boer, L. C. Sime, E. W. Wolff, C. L. Quéré, and L. Bopp (2013), Southern Hemisphere westerly wind changes during the Last Glacial Maximum: Paleo-data synthesis, *Quat. Sci. Rev.*, *68*, 76–95, doi:10.1016/j.quascirev.2013.01.017.
- Köhler, P., H. Fischer, G. Munhoven, and R. E. Zeebe (2005), Quantitative interpretation of atmospheric carbon records over the last glacial termination, *Global Biogeochem. Cycles*, *19*, GB4020, doi:10.1029/2004GB002345.
- Large, W. G., and S. G. Yeager (2008), The global climatology of an interannually varying air sea flux data set, *Clim. Dyn.*, *33*, 341–364, doi:10.1007/s00382-008-0441-3.
- Large, W. G., J. C. McWilliams, and S. C. Doney (1994), Oceanic vertical mixing: A review and a model with a nonlocal boundary layer parameterization, *Rev. Geophys.*, *32*(4), 363–403, doi:10.1029/94RG01872.
- Lee, S.-Y., J. C. H. Chiang, K. Matsumoto, and K. S. Tokos (2011), Southern Ocean wind response to North Atlantic cooling and the rise in atmospheric CO₂: Modeling perspective and paleoceanographic implications, *Paleoceanography*, *26*, PA1214, doi:10.1029/2010PA002004.
- Lippold, J., Y. Luo, R. Francois, S. E. Allen, J. Gherardi, S. Pichat, B. Hickey, and H. Schulz (2012), Strength and geometry of the glacial Atlantic Meridional Overturning Circulation, *Nat. Geosci.*, *5*, 813–816, doi:10.1038/ngeo1608.
- Locarnini, R., A. Mishonov, J. Antonov, T. Boyer, and H. Garcia (2006), *World Ocean Atlas 2005, Volume 1: Temperature*, 182 p., S. Levitus (ed), NOAA Atlas NESDIS 61, U.S. Gov. Printing Office, Washington, D. C.
- Losch, M., D. Menemenlis, J.-M. Campin, P. Heimbach, and C. Hill (2010), On the formulation of sea-ice models. Part 1: Effects of different solver implementations and parameterizations, *Ocean Model.*, *33*, 129–144, doi:10.1016/j.ocemod.2009.12.008.
- Lüthi, D., et al. (2008), High-resolution CO₂ concentration record 650,000–800,000 years before present, *Nature*, *453*, 379–382, doi:10.1038/nature06949.
- Lynch-Stieglitz, J., et al. (2007), Atlantic meridional overturning circulation during the last glacial maximum, *Science*, *316*, 66–69, doi:10.1126/science.1137127.
- Marchal, O., and W. B. Curry (2008), On the abyssal circulation in the glacial Atlantic, *J. Phys. Oceanogr.*, *38*, 2014–2037, doi:10.1175/2008JPO3895.1.
- Marinov, I., A. Gnanadesikan, J. R. Toggweiler, and J. L. Sarmiento (2006), The Southern Ocean biogeochemical divide, *Nature*, *441*, 964–967, doi:10.1038/nature04883.
- Marshall, J., A. Adcroft, C. Hill, L. Perelman, and C. Heisey (1997), A finite-volume, incompressible Navier Stokes model for studies of the ocean on parallel computers, *J. Geophys. Res.*, *102*(C3), 5753–5766.
- Martin, J., G. Knauer, D. Karl, and W. Broenkow (1987), VERTEX: Carbon cycling in the Northeast Pacific, *Deep-Sea Res.*, *34*(2), 267–285, doi:10.1016/0198-0149(87)90086-0.
- Matsumoto, K., and Y. Yokoyama (2013), Atmospheric $\Delta^{14}\text{C}$ reduction in simulations of Atlantic overturning circulation shutdown, *Global Biogeochem. Cycles*, *27*, 296–304, doi:10.1002/gbc.20035.
- Menviel, L., A. Timmermann, A. Mouchet, and O. Timm (2008), Climate and marine carbon cycle response to changes in the strength of the southern hemispheric westerlies, *Paleoceanography*, *23*, PA4201, doi:10.1029/2008PA001604.

- Menviel, L., F. Joos, and S. Ritz (2012), Simulating atmospheric CO₂, ¹³C and the marine carbon cycle during the Last Glacial-Interglacial cycle: Possible role for a deepening of the mean remineralization depth and an increase in the oceanic nutrient inventory, *Quat. Sci. Rev.*, *56*, 46–68, doi:10.1016/j.quascirev.2012.09.012.
- Meredith, M. P., and A. M. Hogg (2006), Circumpolar response of Southern Ocean eddy activity to a change in the Southern Annular Mode, *Geophys. Res. Lett.*, *33*, L16608, doi:10.1029/2006GL026499.
- MITgcm Group (2013), MITgcm user manual, online documentation (http://mitgcm.org/public/r2_manual/latest/online_documents), MIT/EAPS, Cambridge, USA.
- Munday, D. R., H. L. Johnson, and D. P. Marshall (2012), Eddy saturation of equilibrated circumpolar currents, *J. Phys. Oceanogr.*, *43*, 507–532, doi:10.1175/JPO-D-12-095.1.
- Murakami, S., R. Ohgaito, A. Abe-Ouchi, M. Crucifix, and B. L. Otto-Bliesner (2008), Global-scale energy and freshwater balance in glacial climate: A comparison of three PMIP2 LGM simulations, *J. Clim.*, *21*, 5008–5033, doi:10.1175/2008JCLI2104.1.
- Olbers, D., D. Borowski, C. Völker, and J.-O. Wolff (2004), The dynamical balance, transport and circulation of the Antarctic circumpolar current, *Antarct. Sci.*, *16*, 439–470, doi:10.1017/S0954102004002251.
- Otto-Bliesner, B. L., E. C. Brady, G. Clauzet, R. Tomas, S. Levis, and Z. Kothavala (2006), Last Glacial Maximum and Holocene Climate in CCSM3, *J. Clim.*, *19*, 2526–2544, doi:10.1175/JCLI3748.1.
- Otto-Bliesner, B. L., C. D. Hewitt, T. M. Marchitto, E. Brady, A. Abe-Ouchi, M. Crucifix, S. Murakami, and S. L. Weber (2007), Last Glacial Maximum ocean thermohaline circulation: PMIP2 model inter-comparisons and data constraints, *Geophys. Res. Lett.*, *34*, L12706, doi:10.1029/2007GL029475.
- Parekh, P., M. J. Follows, S. Dutkiewicz, and T. Ito (2006), Physical and biological regulation of the soft tissue carbon pump, *Paleoceanography*, *21*, PA3001, doi:10.1029/2005PA001258.
- Parrenin, F., V. Masson-Delmotte, P. Köhler, D. Raynaud, D. Paillard, J. Schwander, C. Barbante, A. Landais, A. Wegner, and J. Jouzel (2013), Synchronous change in atmospheric CO₂ and Antarctic temperature during the last deglacial warming, *Science*, *339*, 1060–1063, doi:10.1126/science.1226368.
- Ritz, S. P., T. F. Stocker, J. O. Grimalt, L. Menviel, and A. Timmermann (2013), Estimated strength of the Atlantic overturning circulation during the last deglaciation, *Nat. Geosci.*, *6*, 208–212, doi:10.1038/nges01723.
- Roche, D., X. Crosta, and H. Renssen (2012), Evaluating Southern Ocean sea-ice for the Last Glacial Maximum and preindustrial climates: PMIP-2 models and data evidence, *Quaternary Sci. Rev.*, *56*, 99–106, doi:10.1016/j.quascirev.2012.09.020.
- Rojas, M., P. Moreno, M. Kageyama, M. Crucifix, C. Hewitt, A. Abe-Ouchi, R. Ohgaito, E. C. Brady, and P. Hope (2009), The Southern Westerlies during the Last Glacial Maximum in PMIP2 simulations, *Clim. Dyn.*, *32*, 525–548, doi:10.1007/s00382-008-0421-7.
- Schmitt, J., et al. (2012), Carbon isotope constraints on the deglacial CO₂ rise from ice cores, *Science*, *336*, 711–714, doi:10.1126/science.1217161.
- Sijp, W. P., and M. H. England (2008), The effect of a northward shift in the Southern Hemisphere westerlies on the global ocean, *Prog. Oceanogr.*, *79*, 1–19, doi:10.1016/j.pocean.2008.07.002.
- Sijp, W. P., and M. H. England (2009), Southern Hemisphere Westerly Wind Control over the Ocean's Thermohaline Circulation, *J. Clim.*, *22*, 1277–1286, doi:10.1175/2008JCLI2310.1.
- Sime, L. C., K. E. Kohfeld, C. L. Quéré, E. W. Wolff, A. M. de Boer, R. M. Graham, and L. Bopp (2013), Southern Hemisphere westerly wind changes during the Last Glacial Maximum: Model-data comparison, *Quaternary Sci. Rev.*, *64*, 104–120, doi:10.1016/j.quascirev.2012.12.008.
- Toggweiler, J. R., J. L. Russell, and S. R. Carson (2006), Midlatitude westerlies, atmospheric CO₂, and climate change during the ice ages, *Paleoceanography*, *21*, PA2005, doi:10.1029/2005PA001154.
- Treguier, A. M., J. Le Sommer, J. M. Molines, and B. de Cuevas (2010), Response of the Southern Ocean to the Southern annular mode: Interannual variability and multidecadal trend, *J. Phys. Oceanogr.*, *40*, 1659–1668, doi:10.1175/2010JPO4364.1.
- Tschumi, T., F. Joos, and P. Parekh (2008), How important are Southern Hemisphere wind changes for low glacial carbon dioxide? A model study, *Paleoceanography*, *23*, PA4208, doi:10.1029/2008PA001592.
- Tschumi, T., F. Joos, M. Gehlen, and C. Heinze (2011), Deep ocean ventilation, carbon isotopes, marine sedimentation and the deglacial CO₂ rise, *Clim. Past*, *7*, 771–800, doi:10.5194/cp-7-771-2011.
- Wei, W., G. Lohmann, and M. Dima (2012), Distinct modes of internal variability in the Global Meridional Overturning Circulation associated with the Southern Hemisphere westerly winds, *J. Phys. Oceanogr.*, *42*, 785–801, doi:10.1175/JPO-D-11-038.1.
- Zhang, X., G. Lohmann, G. Knorr, and X. Xu (2013), Different ocean states and transient characteristic in Last Glacial Maximum simulations and implications for deglaciation, *Clim. Past*, *9*, 2319–2333, doi:10.5194/cp-9-2319-2013.